Materials Transactions, Vol. 49, No. 3 (2008) pp. 605 to 611

Sorption of Co^{2+} Ions on the Biogenic Mn Oxide Produced by a Mn-Oxidizing Fungus, *Paraconiothyrium sp.* WL-2

Keiko Sasaki[1,*], Minoru Matsuda[1], Tomohiro Urata[1], Tsuyoshi Hirajima[1] and Hidetaka Konno[2]

[1]*Department of Earth Resources Engineering, Kyushu University, Fukuoka 819-0395, Japan*
[2]*Graduate School of Engineering, Hokkaido University, Sapporo 060-8628, Japan*

A *Paraconiothyrium sp.* WL-2 of Mn-oxidizing fungus is highly tolerant to Mn^{2+} ions, and capable of oxidizing more than 380 mg dm^{-3} of Mn^{2+} ions, leading to the formation of a large amount of insoluble Mn(III, IV) oxides. The biogenic Mn oxides were characterized by X-ray diffraction, FT-Infrared spectroscopy, elemental analysis, measurement of specific surface area, scanning electron microscopy, and measurement of zeta potential, in comparison with the synthetic Mn oxides. It was found that the biogenic Mn oxide is poorly crystalized birnessite, with higher porosity and much more weakly bounded Mn(II) on the surface than the synthetic Mn oxide. Cobalt(II) ions were sorbed and incorporated as Co(III) into the structure of the biogenic Mn oxide. Sorption efficiency in the biogenic Mn oxide was 5.6 times as high as that in the synthetic ones. Relation of the relased Mn^{2+} ions to the immobilized Co suggested that Mn(IV) is preferentially used as oxidants over Mn(III) in the biogenic Mn oxide, and emphasized that the existence of Mn(III) in the biogenic Mn oxide activates the geochemical cycles of Mn and the other involved elements in environments. [doi:10.2320/matertrans.M-MRA2007888]

(Received May 10, 2007; Accepted October 17, 2007; Published February 6, 2008)

Keywords: *manganese-oxidizing fungus, biogenic manganese oxides, sorption of heavy metals, birnessite*

1. Introduction

Manganese (Mn) is the second most abundant transition metal in the earth's crust where it exists at about 1 g kg^{-1} and with several oxidation states.[1)] The II, III and IV oxidation states of Mn are environmentally important in soils and waters. Manganese(II) ions are mobile under pH values from 6 to 9 in natural water, whereas most transition metal ions are immobilized as hydroxides and oxyhydroxides in a wide pH region from neutral to alkaline. Manganese(II) oxidation in natural water system is thermodynamically favorable but often proceeds at very slow rates in the absence of microorganisms.[2)]

Microorganisms can accelerate the rate of Mn^{2+} oxidation by up to five orders of magnitude compared to abiotic Mn^{2+} oxidation,[3,4)] therefore, the role of Mn-oxidizing microoganisms is regarded to be important in controlling not only Mn cycles but also trace metals and metalloids which are sorbed in soil and water system.[5)] Biogenic Mn oxides are known to participate in a wide variety of redox and sorption reactions with metals and metalloides.[6,7)] Selective dissolution techniques have provided the understanding the trace elements associated with Mn oxides.[8)] Additionally, X-ray absorption near-edge structure (XANES) and extended X-ray absorption fine structure (EXAFS) spectroscopy have contributed to find that there is a variety of sorption mechanism to Mn oxides depending on elements.[9)] For example, Pb^{2+} ions are sorbed to Mn oxides by doublet edge sharing and triplet corner sharing coodination without oxidation, wheras Ce(III) is oxidized to Ce(IV) to be immbilized in marine ferroomanganese oxides.[10)] Cobalt accumulates in soils with high abundances of manganese, and is one of the elements most strongly concentrated in manganese oxides.[11–13)]

Previously we reported that a new Mn-oxidizing fungus was isolated from a constructed wetland in Hokkaido and identified to be closely related to the *Paraconiothyrium sp.*-like strain.[14)] The strain is unique to have high Mn tolerance and oxidize more than 380 mg dm^{-3} of Mn^{2+} ions.[15)] In the present work, the biogenic Mn oxide was produced by the strain of fungus, and characterized chemically, morphologically and mineralogically. Sorption of Co^{2+} ions to the biogenic Mn oxide was investigated and compared with that of the synthetic Mn oxides.

2. Experimental

2.1 Microorganism and the formation of the biogenic Mn oxides

The Mn-oxidizing fungus, a *Paraconiothyrium sp.* WL2, was isolated from a constructed wetland, Kaminokuni Hokkaido, Japan. The fungus was identified morphometrically and genetically using analysis of the sequence in the ITS1-5.8 S rRNA-ITS 2 genes.[14)] The growth medium was prepared by modification of the medium for Mn-oxidizing bacteria, *Leptothrix discophora*, but organic nourishments were used at much reduced concentrations as follows: $MgSO_4 \cdot 7H_2O$ 0.6 g, $CaCl_2 \cdot 2H_2O$ 0.07 g, peptone 0.05 g, yeast extract 0.05 g (PY medium), PIPES (piperazine-N,N′-bis(2-ethane sulfonic acid)) 4.53 g per 1 dm^3 of distilled water. The initial pH was adjusted to 6.6 with 1 mol dm^{-3} NaOH. The optimization of the medium composition for the fungal Mn oxidation was described in details elsewhere.[15)]

A 500 cm^3 Erlenmeyer flask was filled with 150–200 cm^3 of the medium. The concentration of Mn^{2+} was adjusted to $[Mn^{2+}] = 150$ mg dm^{-3}. Finally, 0.5 mg (wet weight) of the strain was inoculated into the medium. The flask was installed in a rotary shaking culture-apparatus TS (Takasugi Kagaku) and the cultures were incubated at 25 ± 2°C and 100 rpm within 2 weeks under light shielding.

After the fungal Mn^{2+} oxidation was completed, the precipitates were collected by filtration with a 5 μm pore size membrane filter, and rinsed with distilled water to remove the adsorbed organic matters and any heavy metal and major ions on the surface of the biogenic Mn oxide. The filtrate was then

*Corresponding author, E-mail address: keikos@mine.kyushu-u.ac.jp

lyophilized by a freeze-drier FD-5N (EYELA, Japan) for 24 h, and stored at 4°C prior to metal sorption experiments.

For comparison with the biogenic Mn oxide, the synthetic Mn oxide was chemically produced. The Mn(II) oxidation at neutral pHs by usual oxidants, such as O_2 and H_2O_2, is not significant, therefore, ammonium peroxodisulfate was used as an oxidant in this study. First, a 18.2 mol dm^{-3} of $MnSO_4 \cdot 5H_2O$ (1000 g dm^{-3} Mn) was heated to boiling, and 18.2 mol dm^{-3} of ammonium peroxodisulfate was added gradually to the boiling Mn^{2+} solution, forming blackish and fine particulate precipitates. After cooling the solution containing the synthetic Mn oxide, the precipitates were collected by filtration to be freeze-dried in the same manner as for the biogenic Mn oxide.

2.2 Characterization of the biogenic Mn oxides

The biogenic and synthetic Mn oxides were characterized by X-ray diffraction (XRD), Fourier transformed infrared (FTIR) spectroscopy, scanning electron microscopic observation (SEM), and measurement of specific surface area. XRD measurements for the biogenic and the synthetic Mn oxides were carried out with an XRD Multi Flex (Rigaku, Japan) using CuKα radiation at 20 mA and 40 kV. The FTIR spectra for biogenic and synthetic Mn oxides were collected in a region of 4000 cm^{-1} to 400 cm^{-1} with a JASCO FT/IR 670 plus using diffusion reflectance infrared Fourier transformed method (DRIFT) after 5.0(w/w)% dilution in KBr powder. The morphologies of the biogenic and synthetic Mn oxides were observed using a SS-550 SEM (Shimadzu, Japan) at an acceleration voltage of 15 kV after evaporating a thin platinum/gold layer on the samples. The specific surface area was determined by the seven-point N_2-adsorption BET method, and the pore-distribution was also determined by the BJH method using a BELLSORP-mini (BELL Inc., Japan). The zeta potentials were measured for the biogenic and synthethic Mn oxides by a Zeecom ZE-2000 under $[KNO_3] = 1$ mmol dm^{-3}. Elemental compositions in the biogenic and synthetic Mn oxides were determined for Mn by an ICP-AES and for the involved alkaline and alkaline earth metals by a Thermo SOLAA atomic adsorption spectrometry (AAS) after decomposition in 6 mol·dm^{-3} HCl. Additionally both were extracted in 50 mmol dm^{-3} $CuSO_4$ for 12 h at 25°C to evaluate the contents of weakly bounded Mn(II) species. For the biogenic Mn oxide, organic fractions were estimated by weight differences after combusion at 500°C.

2.3 Sorption of Co^{2+} ions on biogenic Mn oxides

Sorption experiments on the biogenic and synthetic Mn oxides were conducted as follows: 0.020 g of freeze-dried biogenic Mn oxides and 0.015 g of freeze-dried synthetic Mn oxide powders were suspended into the 0.150 dm^3 of up to 175 µmol dm^{-3} $Co(NO_3)_2 \cdot 6H_2O$ in 500 dm^3 Erlenmeyer flasks under the constant ionic strength with 100 mmol dm^{-3} KNO_3, and the flasks were capped with rubber stoppers. Under the condition, solid Mn concentration corresponds to 1 mmol dm^{-3} Mn in the biogenic and synthetic Mn oxides. For the control, Co^{2+} sorption on the fungal tissue was also conducted. Instead of the biogenic Mn oxide, only fungal tissue with the same amount as in the biogenic Mn oxide used was added into the Co^{2+} solution. The initial pH of the Co^{2+} solution buffered using PIPES was 6.5. The flasks were installed on a reciprocal shaker at 25°C and 100 rpm for 100∼300 h. At intervals, the supernatants were sampled and filtered by a 0.2 µm membrane filter for determination of the residual Co^{2+} and released Mn^{2+} concentrations in the solution using an atomic absorption spectrometry and induced coupled plasma mass spectrometry (ICP-MS, Agilent 7500c). The detection limits in AAS and ICP-MS are 1.4 µg dm^{-3} and 0.06 µg dm^{-3} for Mn, and 6.0 µg dm^{-3} and 0.01 µg dm^{-3} for Co. Finally, the precipitates were collected by filtration using a membrane filter of 5.0 µm pore size, thoroughly air-dried for one week at 4°C.

To investigate the chemical states of Mn and Co in the precipitates, XP-spectra for the biogenic Mn oxide after and before Co sorption were collected by an AXIS 165 (Shimadzu, Japan). After evacuating to less than 10^{-7} Torr for more than 60 min, the sample was transferred into an analyzer chamber at less than 10^{-10} Torr, and then irradiated with monochromized Al Kα X ray (15 kV, 7 mA) using a neutrilizer. The binding energy, E_B, was calibrated with E_B[C 1s] = 284.5 eV. Data were analyzed with CASAXPS software. Backgrounds were drawn using the Shirley method. The obtained spectra were curve-fitted using Gaussian-Lorentzian mixed functions.

3. Results and Discussion

3.1 Characterization of the biogenic Mn oxides

Figure 1 shows the XRD patterns of the biogenic and synthetic Mn oxides. The XRD pattern of the biogenic Mn oxide (Fig. 1(a)) has a noisy background with an ambiguous

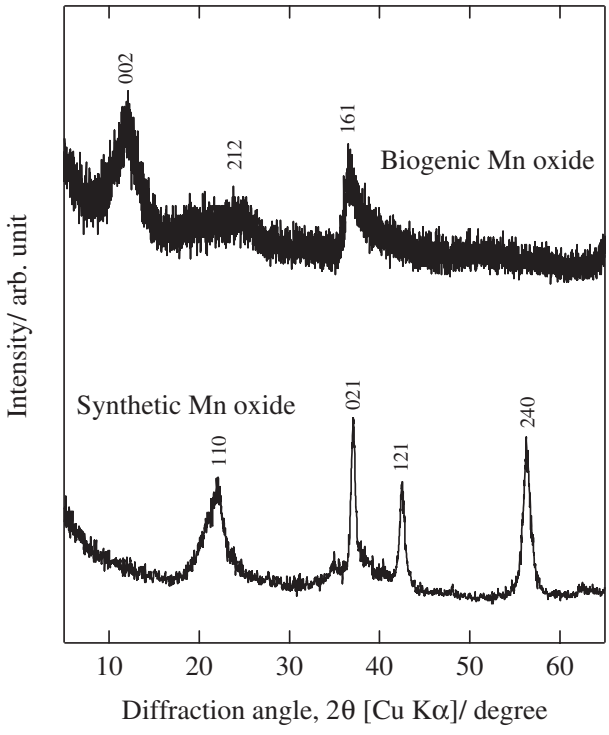

Fig. 1 The XRD patterns of the (a) biogenic and (b) synthetic Mn oxides. Miller indices are shown as (a) birnessite ($Na_4Mn^{(III)}{}_6Mn^{(IV)}{}_8O_{27} \cdot 9H_2O$, JCPDS 23-1046), and (b) ramsdellite (γ-MnO_2, JCPDS 7-222).

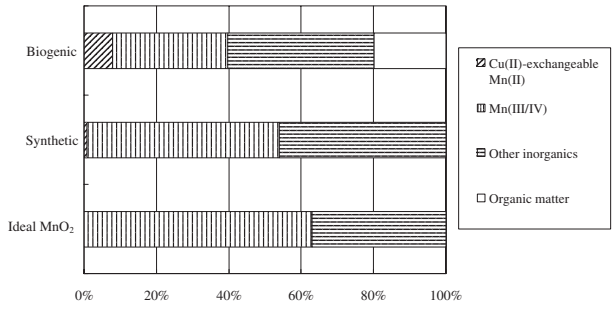

Fig. 2 Chemical compositions of the biogenic and synthetic Mn oxides.

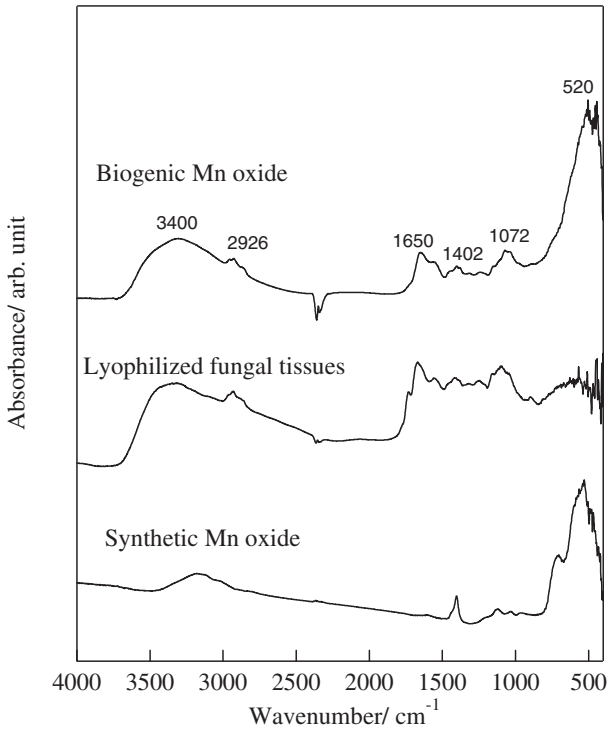

Fig. 3 FTIR spectra for biogenic Mn oxide and the related substances.

and broad peak and two relatively sharp peaks, indicating that it is poorly crystalline, typical of most bio-minerals. Two peaks at around $2\theta = 12^\circ$ and 37° are assigned to 002 and 161 of birnessite ($Na_4Mn^{(III)}{}_6Mn^{(IV)}{}_8O_{27}\cdot 9H_2O$, JCPDS 23-1046), a broad peak near $2\theta = 20$–25° can be tentatively assigned to 212 of birnessite in Fig. 1(a). Although these assignments might not be definite, the biogenic Mn oxide contains birnnesite primarily, and the chemical forms of Mn in the biogenic Mn oxide is thought to be Mn(III) and Mn(IV) which were formed by fungal Mn-oxidation. It is reported that the fungal oxidation of Mn produces Mn(III) directly by enzymatic reaction, but not Mn(IV). Instead, Mn(IV) is formed by disproportionation of Mn(III).[16] If the disproportionation is not complete, Mn(III)-species are also involved in the biogenic precipitates. In contrast, the XRD pattern for the synthetic Mn oxide has a low-noise background and four distinctive peaks at $2\theta = 22^\circ$, 37°, 42° and 56° as shown in Fig. 1(b). Respectively, these peaks are assigned to 110, 021, 121, and 240 of ramsdellite (γ-MnO_2, JCPDS 7-222). It is reasonable that the crystalline phase of the synthetic Mn oxide consists of ramsdellite.

The Mn contents were determined to be 39.2 (w/w)% and 54.1 (w/w)% in the biogenic and synthetic Mn oxides, including 7.4 and 0.75% of Cu-exchangeable Mn(II), which is named as weakly bounded Mn(II). The biogenic Mn oxides includes around 20% of organic matters (Fig. 2). According to trace elemental analysis of the biogenic Mn oxides, it was found that 0.48 (w/w)% K was involved and Ca and Mg were not detected. Probably H^+ and Mn^{2+} would compensate the charge balance in the structure.

As shown in Fig. 3, FT-IR spectrum for the biogenic Mn oxides showed a distinct peak at 520 cm^{-1} corresponding to Mn-O stretching vibration mode in Mn oxides,[17] which can be observed also in the synthetic Mn oxides. Additionally, there are relatively small peaks from the fungal tissues: two peaks at 1072 cm^{-1} and 1402 cm^{-1} corresponding to stretching vibration mode of oxyanion like sulfonic groups, a peak at 1650 cm^{-1} corresponding to C=O stretching vibration mode of carboxylic group, a peak at 2926 cm^{-1} corresponding to C-H stretching vibration mode of methylamine groups, and a broad peak around 3400 cm^{-1} corresponding to O-H stretching vibration mode of water molecules. FT-IR data supports that the biogenic Mn oxides involves fragments in proteins and polysaccharides from the fungal tissues, which might participate in sorption of positive and negative charged trace elements in environments.

Figure 4(a) shows SEM image of the biogenic Mn oxides, which looks like the aggregated framboidal and porous particles with several micrometers in diameter, and has the mark of hyphae in the fungal organs, something like a broken tube around the center. The size and shape of the biogenic Mn oxide particles were not uniform. On the other hand, the morphology of the synthetic Mn oxide particles is mostly uniformed spheres with 1–1.5 μm in diameter as shown in Fig. 4(b). These SEM observations showed that the morphology of the biogenic and synthetic Mn oxides is significantly different each other.

The specific surface area of the biogenic Mn oxide was determined to be 81.4 $m^2\,g^{-1}$, which is much larger than the 11.3 $m^2\,g^{-1}$ surface area of the synthetic one. Although the biogenic Mn oxide is actually a mixture of inorganic Mn deposits and lyophilized fungal tissues, the specific surface area of fungal substances was observed to be 4.3 $m^2\,g^{-1}$, indicating the minimal contribution of fungal substances to the surface areas of the biogenic Mn oxide.[18] Figure 5 shows distributions of pore size in the biogenic and the synthetic Mn oxides. The biogenic Mn oxide has uniformly nanometer-sized structure, with pores predominantly around 4 nm diameter, whereas the synthetic Mn oxide has a less distinctive trend in pore distribution. The higher density of fine pores in the biogenic Mn oxide gives it a larger specific surface than that of the synthetic Mn oxide.

The zeta potentials for the biogenic and synthetic Mn oxides were measured at different pHs as shown in Fig. 6. The zero points of charge were 2.7–2.8 for both. There is a number of the previously reported data of ZPC for Mn oxides with a wide range from 1.5 to 7.7 determined using titration and electrophoresis,[19–24] probably depending on the preparation and high surface reactivity.

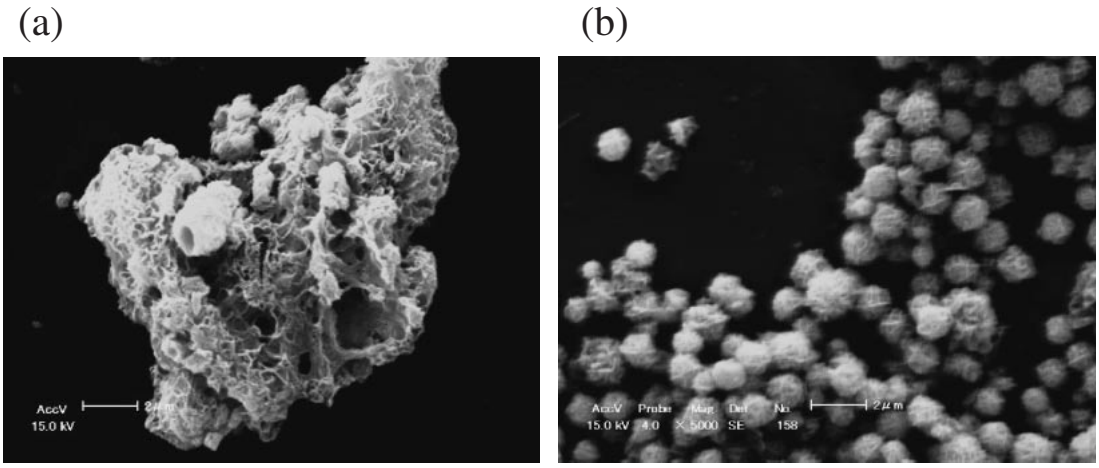

Fig. 4 SEM images of the (a) biogenic and (b) synthetic Mn oxide. The horizontal bars indicate 2 μm in (a) and (b).

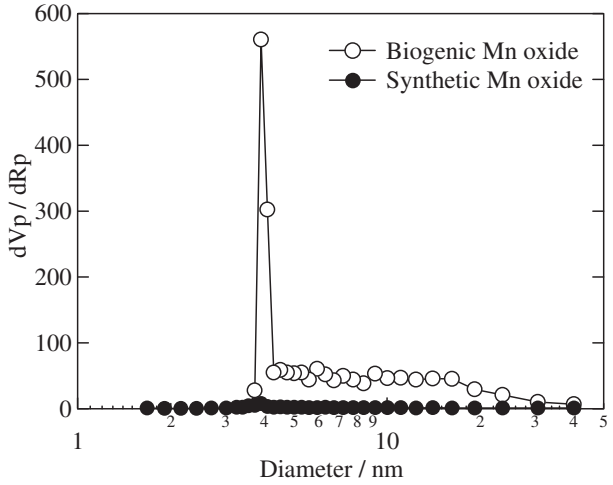

Fig. 5 Pore size distributions of the biogenic and synthetic Mn oxides. Vp: volume of particle pores; Rp: radius of particles pores.

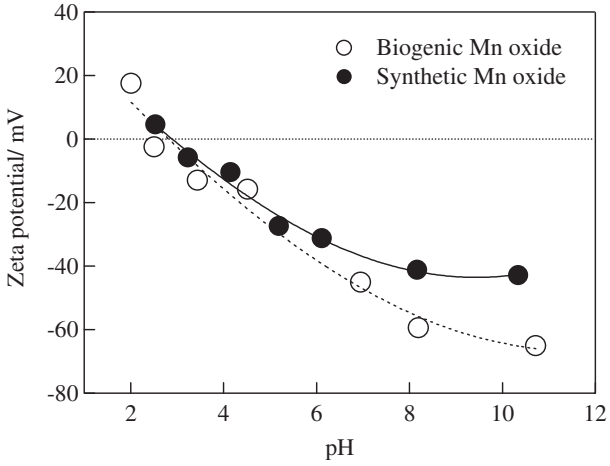

Fig. 6 Zeta potentials of the biogenic and synthetic Mn oxides with pHs.

3.2 Sorption of Co(II) to the biogenic Mn oxides

There was a large difference in Co-sorption behaviour between the biogenic and synthetic Mn oxides. Figure 7 shows the time cources in residual Co^{2+} concentrations during Co-sorption at 25°C in duplicate. No sorption of Co^{2+} on the fungus without biogenic Mn oxide was observed. This is consistent with the results concluded by Toner *et al.*[25] in which biogenic functional groups present in the biofilm did not intervene in metal sorption by the biogenic Mn oxide. With the biogenic Mn oxide, the Co concentration dramatically decreased to less than 0.13 mmol dm^{-3} within 24 h, and it took more than 100 h to reach the equibrium concentratin which was 0.09 mmol dm^{-3} (Fig. 7(a)). On the contrary, the synthetic Mn oxide decreased Co concentration to the equibrium value within less than 24 h, which was around 0.15 mmol dm^{-3} (Fig. 7(b)). Based on the Mn contents in Fig. 2, Co^{2+} sorption efficiencies are calculated to be 160 and 28.7 mmol-Co/mol-solid Mn respectively for the biogenic and synthetic Mn oxides. In case of the initial $[Co^{2+}] = 0.55$ mmol dm^{-3}, the similar Co^{2+} sorption efficiency was observed. The value of molar ratio Co/Mn (0.16) for the biogenic Mn oxides was close to the ratio (0.18) of vacancies per octahedral sites in Mn octahedral layer site of the biogenic Mn oxide produced by a Mn-oxidizing bacterium, *Psudomonas putida*,[26] indicating the octahedral vacant sites are responsible to Co-sorption in the biogenic Mn oxide. Thus the Co-sorption efficiency of the biogenic Mn oxide is 5.6 times higher than that of the synthetic Mn oxide. When Co^{2+} sorption equilibrium on the biogenic and synthetic Mn oxides were achieved, the final pHs of the solution were 6.3 and 6.4, respectively. In these pHs the surface charge of Mn oxide is still negative, and sorption of Co^{2+} ions is favourable on Mn oxides. The biogenic Mn oxide has much larger capacity for Co^{2+} sorption than does the synthetic Mn oxide. During Co^{2+} sorption on the biogenic Mn oxide, release of Mn^{2+} was observed with closed symbols in Fig. 8(a). Since Mn^{2+} release was also observed in the absence of Co^{2+} ion, Mn^{2+} release is not always caused by interaction of Co^{2+} with the biogenic Mn oxide. However, in the presence of Co^{2+} ions the excessive release of Mn^{2+} was observed compared with those from the biogenic Mn oxides in the absence of Co^{2+}. On the contrary, in the synthetic Mn oxide, the difference was negligibly small as shown in Fig. 8(b), and the amounts of released Mn were much smaller than in the biogenic Mn oxide. Since the biogenic Mn oxide is poorly crystalline and rich in nanosized fine pores, a part of Mn^{2+}

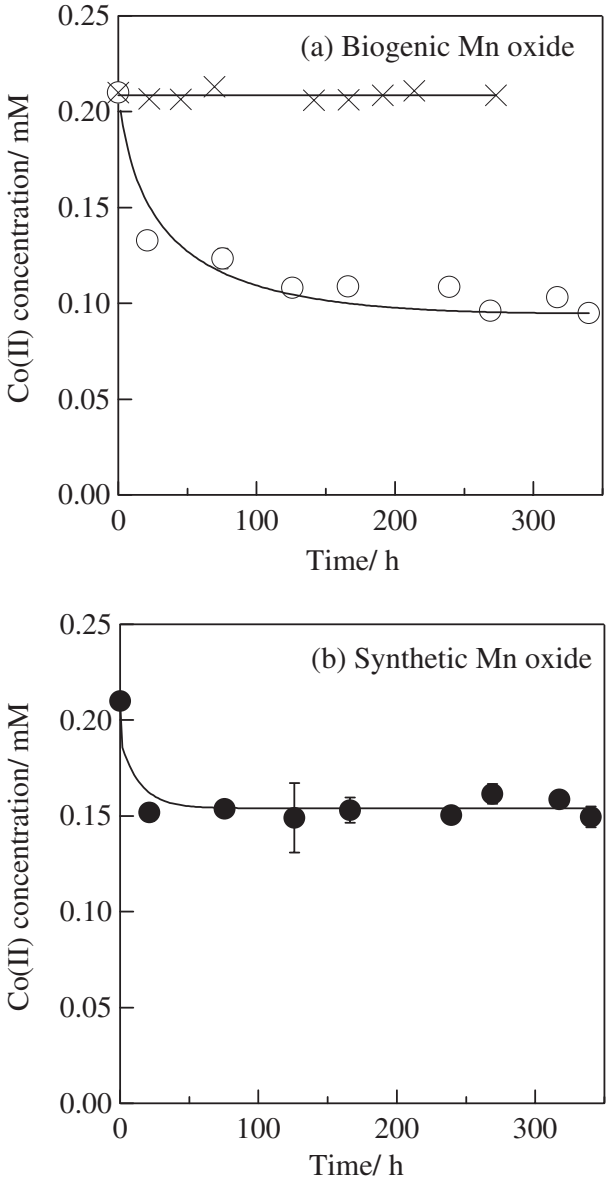

Fig. 7 Sorption behaviour of Co^{2+} ions on (a) the biogenic Mn oxide (○) and the corresponding amounts of lyoplilized fungus (×) to the used fungal tissues in the biogenic Mn oxide, and (b) the synthetic Mn oxides at 25°C.

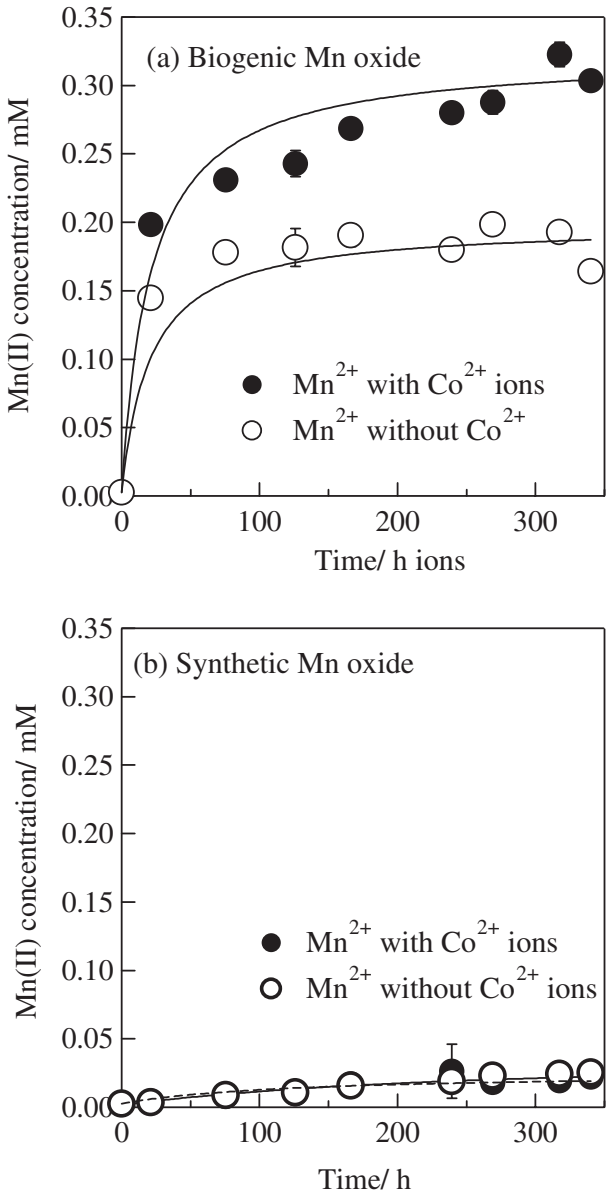

Fig. 8 Changes in the released Mn^{2+} ions with time with the biogenic Mn oxides (a), and the synthetic Mn oxide (b) in the presence of Co^{2+} (closed symbols) and in the absence of Co^{2+} (opened symbols).

ions are loosely involved in the structure (Fig. 2) sometimes to compensate the charge balance, therefore, diffused to the aqueous phase during the shaking, independent of the existence of competively adsorptive species as shown with open symbols in Fig. 8(a).

XP-spectra of Mn 3s and Co 2p regions for the biogenic and synthetic Mn oxides after Co-sorption are shown in Figs. 9 and 10. In Fig. 9(a), (b), the binding energies of Mn 3s, E_B[Mn 3s], are 84.4 eV and 84.0 eV, and the splitting between the Mn 3s peak and the satellite peak are 4.8 eV and 4.6 eV for the biogenic and synthetic Mn oxides respectively, suggesting the predominant existence of Mn(IV) in both oxides.[27] Recent applications of high resolution electron microscopy, time-flight neutron diffraction and synchrotron-based X-ray spectroscopy have led breakthroughs in characterization of the biogenic Mn mineralogy.[28] The splittings were mostly same before and after Co^{2+} sorption (Fig. 9(c)), but clearly different in $MnSO_4$ (Fig. 9(d)). In Fig. 10(a), the Co 2p spectrum has a couple of peaks at E_B[Co $2p_{3/2}$] = 780.0 eV and E_B[Co $2p_{1/2}$] = 795.0 eV without satellites, indicating the existence of Co(III) on the surface of biogenic Mn oxides after sorption of Co^{2+}.[29] In Co 2p spectrum for $CoSO_4$, there is satellite peaks as shown with arrows in Fig. 10(d). This is an evidence that redox reaction occurred between sorbed Co(II) and the biogenic Mn oxides.

The intensity of Co 2p was apparently much larger in the synthetic Mn oxide than in the biogenic one as shown in Fig. 10(a) and (b). The signal at higher binding energies in the Mn 2s region overlapped the tailing of lower binding energies in Co 2p region. This interference by broad peaks of Mn 2s hinders precise determination of the peak intensity of Co $2p_{3/2}$. In the present work, the peak intensity of Co $2p_{1/2}$ is used for the further analysis. Using the relative sensitivity factor of s_{Co2p}/s_{Mn2p}, which was determined to be 1.32 by

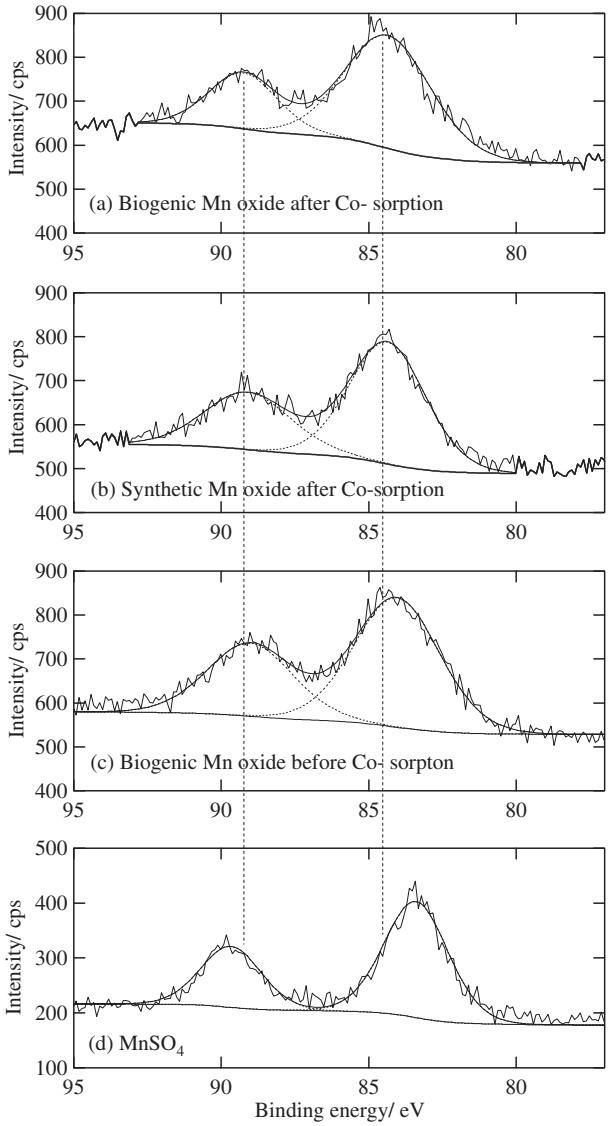

Fig. 9 XP-spectra of the Mn 3s region for the biogenic Mn oxides after Co-sorption (a), and the related samples: (b), synthetic Mn oxides after Co sorption; (c), biogenic Mn oxides before Co sorption; (d) $MnSO_4$ (WAKO special grade reagent). The spectra were separated into Mn 3s peak and satellite using Gaussian-Lorentzian mixed functions.

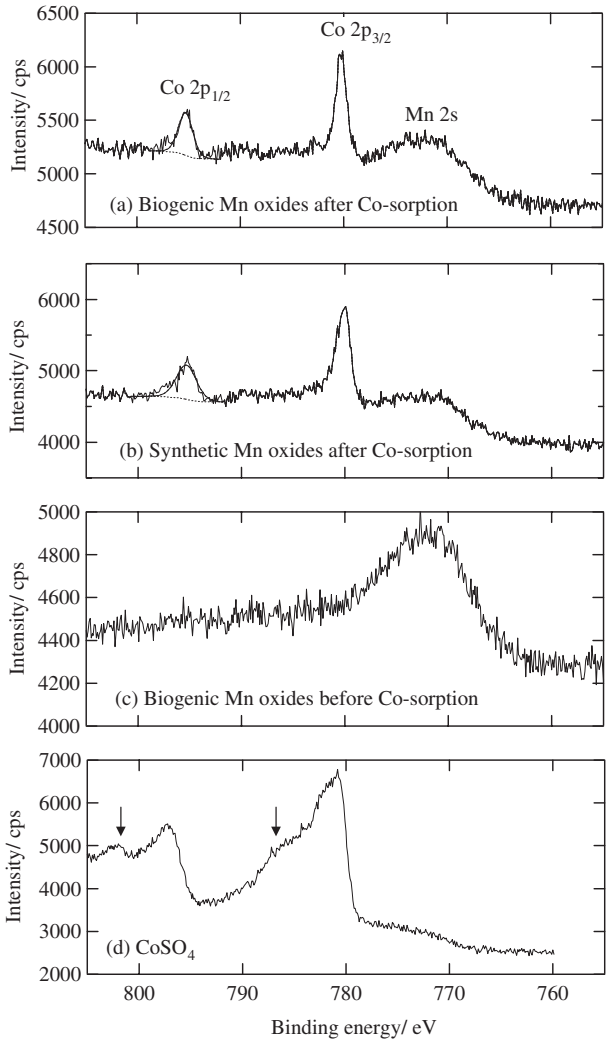

Fig. 10 XP-spectra of the Co 2p-Mn 2s regions for the biogenic Mn oxide after Co-sorption (a), and the related samples: (b), sythetic Mn oxides after Co sorption; (c), biogenic Mn oxides before Co sorption; (d) $CoSO_4$ (WAKO special grade reagent). Arrows indicate the satellite peaks of Co 2p in (d).

measurements of $MnSO_4$ and $CoSO_4$, the mole ratio of n_{Co}/n_{Mn} were evaluated to be 0.070 and 0.115 in the biogenic and synthetic Mn oxides after Co-sorption. It means that the coverage of Co on the Mn oxides was larger in the synthetic Mn oxide than in the biogenic Mn oxide, while the Co^{2+} sorption efficiency was higher in the latter than in the former. The results are reasonable, since much more Co^{2+} ions are considered to penetrate into fine and deep pores in the biogenic Mn oxide which has the larger specific surface area and much more fine pores as shown in Fig. 5.

Apparently the process of Co-immobilization in Mn oxide requires electron transfer from Co(II) to Mn oxides. When Mn(IV) is a sole electron acceptor for Co(III) in the redox process, Mn(III) is generated to associate with the solid phase as shown in the following equations.

$$\text{Co(II)-ads} = e^- + \text{Co(III)-ads}$$
$$\text{Mn(IV)-solid} + e^- = \text{Mn(III)-solid}$$

Based on Figs. 7 and 8, the relationship of released amounts of Mn^{2+} ions through the redox reaction against removed amounts of Co^{2+} ions was depicted in Fig. 11. The values of vertical axis indicate the released amounts of Mn^{2+} ions, excluding simply released Mn^{2+} ions, that is, from the vertical difference between open and closed symbols in Fig. 8. In case of the synthetic Mn oxide, the relation is mostly distributed on the horizontal axis indicating that Mn(IV) is a sole electron acceptor. On the contrary, the biogenic Mn oxides has a different trend in which the relation is distributed between solid and dashed lines. In Fig. 11, the solid line indicates that Mn(III) is a sole electron acceptor to Co^{2+} ions, and a dashed line indicates Mn(III) and Mn(IV) evenly function. That is, with the biogenic Mn oxides Mn(III) serves as an electron acceptor to release Mn^{2+} ions as follows.

$$\text{Co(II)-ads} = e^- + \text{Co(III)-ads}$$
$$\text{Mn(III)-solid} + e^- = \text{Mn(II)}$$

According to the results, Mn(III) in the biogenic Mn oxide is

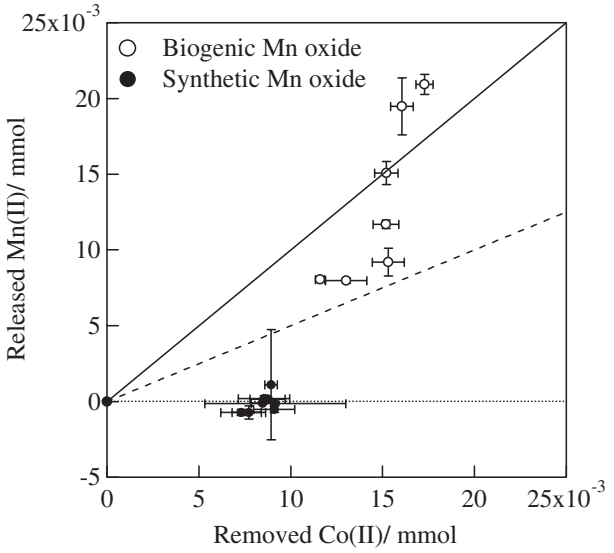

Fig. 11 Interrelationship of the released Mn^{2+} by interaction of Mn oxides with Co^{2+} ions against the removal Co^{2+} ions. The y-axis values are from the difference between with and without Co^{2+} in Fig. 8.

more likely electron sink for oxidation of Co^{2+} preferentially over Mn(IV). This is consistent with the mechanism of Co(II) oxidation by phyllomanganate buserite with 1 nm interlayer spacing using power and polarized EXAFS spectroscopy by Manceau *et al.*[30] Extraction of the residual Mn oxides after Co-sorption in 50 mmol dm^{-3} $CuSO_4$ showed that around 14(w/w)% of exchangeable Co(II) is involved in biogenic and synthetic Mn oxides each. This suggests that sorption of Co^{2+} to Mn oxides proceeds by two steps of adsorption and oxidation through the interlayer in the structure to support the high affinity. It can be expected that Mn(III) species in the biogenic Mn oxides play an important role to control the mobility of trace elements in redox reaction on the interface of aqueous/solid phases in environments.

4. Conclusions

The biogenic Mn oxide produced by a *Paraconiothyrium sp.* WL-2 was characterized to be highly porous with a narrow pore size distribution, having the maximum frequency of pore at 4 nm in diameter. The biogenic oxide is poorly crystalline, and has a specific surface area of 81.4 m^2g^{-1}. Synthetic Mn oxides have a less distinct pore size distribution and much smaller specific surface area. The present experiments with the sorption of Co^{2+} showed that the biogenic Mn oxide has high efficiency for the sorption of heavy metals and around five times higher capacity than the synthetic Mn oxide. This suggests that the biogenic Mn oxide might contribute to the scavenging of heavy metals in natural soils and waters, and that biofilms made using Mn–oxidizing fungi can be exploited for treatment of waste waters impacted by heavy metals.

Acknowledgement

Financial support was provided by the Grant-in-Aid for Scientific Research (B) (No. 16360445) from Japan Society for the Promotion of Science (JSPS). We are indebted to Dr. Yoshinori Miura at the Center of Advanced Instrumental Analysis, Kyushu University for the measurement of XPS.

REFERENCES

1) V. M. Goldschmidt: *Geochemistry*. (Oxford University Press, London, 1958) p. 621–642.
2) K. H. Nealson, B. M. Tebo and R. A. Rosson: Adv. Appl. Microbiol. **33** (1988) 279–318.
3) B. M. Tebo: Deep-Sea Res. **38** (Suppl. 2) (1988) S883–S905.
4) B. Wehrli, G. Friedle and A. Manceau: Reaction rates and products of manganese oxidation at the sediment-water interface. In C. P. Huang, C. O. Melia and J. J. Morgan, Eds., Aquatic Chemistry, **244**, pp. 111–134. Advances in Chemistry Series, American Chemical Society, Washington, D.C. (1995).
5) B. M. Tebo, H. A. Johnson, J. K. McCarthy and A. S. Templeton: TRENDS in Microbiology **13** (2005) 421–428.
6) Y. M. Nelson, L. W. Lion, W. C. Ghiorse and M. L. Shuler: Appl. Environ. Micobiol. **65** (1999) 175–180.
7) B. M. Tebo, J. R. Barger, B. G. Clement, G. J. Dick, K. J. Murray, D. Parker, R. Verity and S. M. Webb: Annu. Rev. Earth Planet. Sci. **32** 287–328.
8) A. Neaman, F. Mouélé, F. Trolard and G. Bourrié: Applied Geochemistry, **19** (2004) 973–979.
9) M. Villabos, Bargar and G. Sposito: Environ. Sci. Technol. **39** (2005) 569–576.
10) Y. Takahashi, A. Manceau, N. Geoffroy, M. A. Marcus and A. Usui: Geochim. Cosmochim. Acta **71** (2007) 984–1008.
11) R. G. Burns: Geochim. Cosmochim. Acta **40** (1976) 95–102.
12) A. Manceau, S. Llorca and G. Calas: Geochim. Cosmochim. Acta **51** (1987) 105–113.
13) J. T. Kay and M. H. Conklin: Environ. Sci. Technol. **35** (2001) 4719–4725.
14) K. Takano, Y. Itoh, T. Ogino, K. Kurosawa and K. Sasaki: Limnology **7** (2006) 219–223.
15) K. Sasaki, M. Matsuda, T. Hirajima, K. Takano and H. Konno: Mater. Trans. **47** (2006) 2457–2461.
16) J. Perez and T. W. Jefferies: Appl. Environ. Microbiol. **58** (1992) 2401–2409.
17) S. J. Parikh and J. Chorover: Geomicrobiol. J. **22** (2005) 207–218.
18) Y. Tani, M. Ohashi, N. Miyata, H. Seyama, K. Iwahori and M. Soma: J. Environ. Sci. Health **39** (2004) 2641–2660.
19) B. Prélot, C. Poinsignon, F. Thomas, E. Schouller and F. Villiéras: J. Colloid and Interface Sci. **257** (2003) 77–84.
20) H. Tamura, T. Oda, M. Katayama and R. Furuichi: Environ, Sci. Technol. **30** (1996) 1198–1204.
21) D. W. Fuerstenau and J. Shibata: Int. J. Miner. Process. **57** (1999) 205–217.
22) T. W. Healy, A. P. Herring and D. W. Fuerstenau: J. Colloid Interface Sci. **21** (1966) 435–444.
23) J. W. Murray: Geochim. Cosmochim. Acta **39** (1975) 635–647.
24) A. Carre, F. Roger and C. Varinot: J. Colloid Interface Sci. **154** (1990) 174–183.
25) B. Toner, A. Manceau, S. M. Webb and G. Sposito: Geochim. Cosmochim. Acta **70** (2006) 27–43.
26) M. Villabos, B. Lanson, A. Manceau, B. Toner and G. Sposito: Amer. Mineral. **91** (2006) 489–502.
27) J. J. Junta and M. F. Jr. Hochella: Geochim. Cosmochim. Acta **58** (1994) 4985–4999.
28) M. Villabos, B. Toner, J. Bargar and G. Sposito: Geochim. Comochim. Acta **67** (2003) 2649–2662.
29) Y. Okamoto, H. Nakano, T. Imanaka and S. Teranishi: Bull. Chem. Soc. Jpn. **48** (1975) 1163–1168.
30) A. Manceau, V. A. Drits, E. Silverster, C. Bartoli and B. Lanson: Am. Mineral. **82** (1997) 1150–1175.